

Supporting Information for

# Time-resolved Impulsive Stimulated Raman Spectroscopy with Synchronized Triple Mode-locked Lasers

**JunWoo Kim,<sup>†</sup> Tai Hyun Yoon<sup>†,‡</sup>, and Minhaeng Cho<sup>†,§</sup>**

<sup>†</sup>Center for Molecular Spectroscopy and Dynamics, Institute for Basic Science (IBS), Seoul 02841, Republic of Korea

<sup>‡</sup>Department of Physics, Korea University, Seoul 02841, Republic of Korea

<sup>§</sup>Department of Chemistry, Korea University, Seoul 02841, Republic of Korea

## 1. Experimental Setup

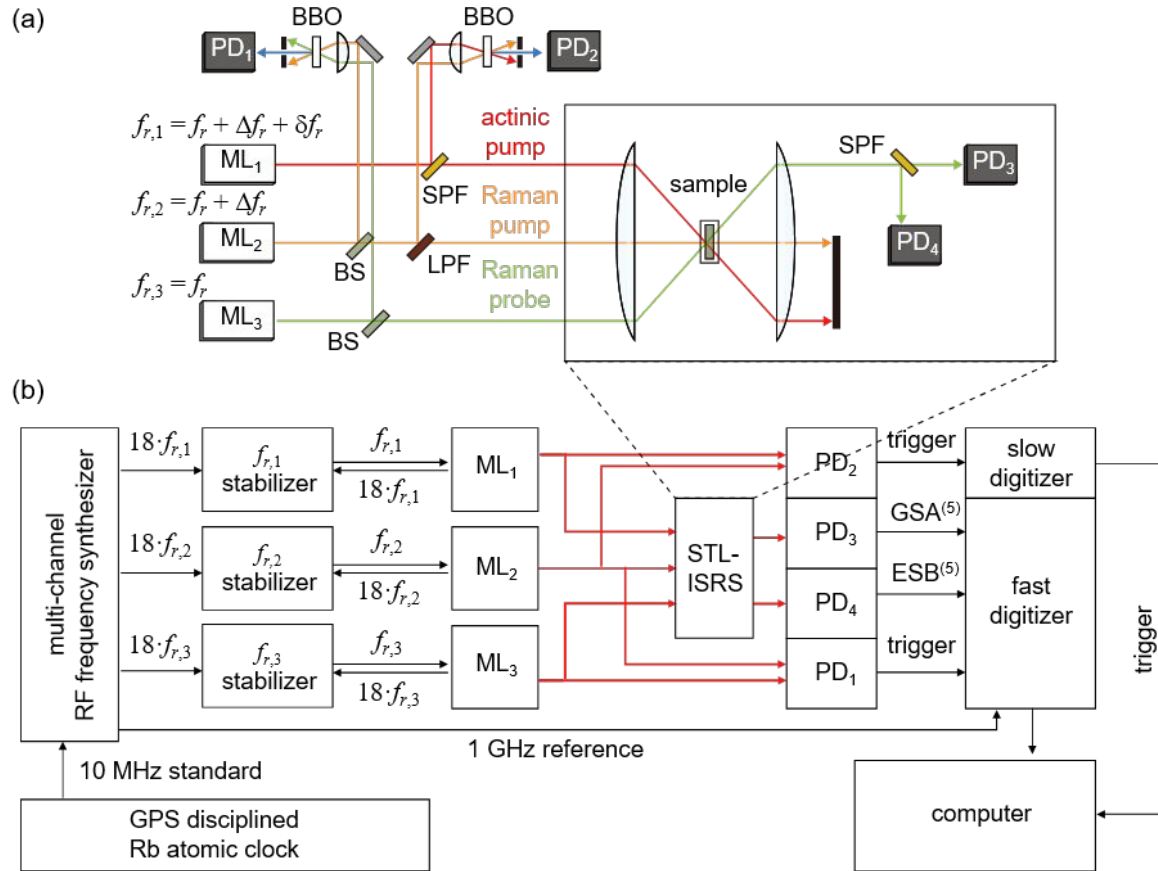


**Figure S1.** (a) Optical layout of STL-ISRS. PD: photodiode, BBO: beta-barium borate crystal, ML: mode-locked laser, BS: beam splitter, SPF: short-pass filter, LPF: long-pass filter,  $f_{r,i}$ : repetition rate of  $i$ th ML. (b) Signal detection and triggering scheme of the STL-ISRS.

Figure S1 depicts the optical layout (a) and its signal detection and triggering scheme (b) of the proposed synchronized triple mode-locked laser-based time-resolved impulsive stimulated Raman spectroscopy (STL-ISRS), where three synchronized mode-locked lasers (MLs) with precisely detuned repetition rates are employed. The trains of pulses from the ML<sub>1</sub>, ML<sub>2</sub>, and ML<sub>3</sub> with variable repetition periods are used as an actinic pump, a Raman pump, and a Raman probe, respectively. The differences in the repetition rates of the three MLs should be precisely controlled because they determine the optical time-delay  $t_1$  between the actinic and Raman pump pulses and the time-delay  $t_2$  between the Raman pump and Raman probe pulses. Such an automatic time-delay scan achieved by employing two repetition-rate-stabilized mode-locked lasers is known as asynchronous optical sampling (ASOPS). Our experimental scheme in Figure

S1 employs two sequential ASOPS measurements by setting the repetition rates of the three MLs properly differently (see Supporting information 2 for details).

The optical layout of our STL-ISRS (Figure S1) is relatively simple compared to the conventional femtosecond stimulated Raman spectroscopy (FSRS) and TR-ISRS systems due to the absence of long mechanical delay lines and wavelength conversion optics. To carry out the STL-ISRS experiments with the setup shown in Figure S1, we need to separately use the high- and low-frequency parts of the broad power spectra of the ML<sub>1</sub> and ML<sub>2</sub>. Note that the spectral bandwidth of each ML is as broad as 3000 cm<sup>-1</sup> (see Figure 2a in the main text). We use a short-pass filter to produce the actinic pump pulses from ML<sub>1</sub>. A long-pass filter after ML<sub>2</sub> is used to produce the Raman pump pulses. Note that the Raman pump beam is deliberately made to be electronically non-resonant with the quantum transition between the ground and excited states of molecules at the thermal equilibrium state. That is to say, only the short-pass filtered pulses from ML<sub>1</sub> not the long-pass filtered pulses from ML<sub>2</sub> act as the actinic pump (Figures 1d and S1a). The repetition rates of the three MLs are different from one another as  $f_{r,1} = f_r + \Delta f_r + \delta f_r$ ,  $f_{r,2} = f_r + \Delta f_r$  and  $f_{r,3} = f_r$ , where  $f_r = 80.0$  MHz. In the present work, we precisely set the two detuning frequencies  $\Delta f_r$  and  $\delta f_r$  to be 38.4 Hz, and 77 mHz, respectively. Here, each repetition rate ( $f_{r,i}$ ) is phase-locked in such a way that its eighteenth harmonics ( $18f_{r,i}$ ) is referenced to the RF frequency generated from a multi-channel RF frequency synthesizer (Holzworth, HS9008A). The time-base of the frequency synthesizer is phase-locked to the standard frequency of a GPS disciplined Rb atomic clock at 10 MHz (Figure S1b). The remarkable stability of the synchronized repetition rates of the three MLs that are controlled by the atomic clock enables one to accurately and precisely control the two pulse-to-pulse delay times,  $t_1$  and  $t_2$ .<sup>1</sup> This ASOPS scheme for the automatic time scanning of the waiting time  $t_1$  is critical for the long-term monitoring of photochemical reactions of interest.<sup>2</sup>

The actinic pump, Raman pump, and Raman probe beams are focused at the sample by using an off-axis parabolic mirror ( $f = 10$  cm). The pulse energies of the actinic pump from ML<sub>1</sub> and the Raman pump from ML<sub>2</sub> are 1.2 and 1.5 nJ, respectively, right before the sample, while the pulse energy of the Raman probe from ML<sub>3</sub> is less than 0.1 nJ. The Raman probe beam after the sample carries information on the nonlinear optical responses from the dye molecules in solutions, and a dichroic mirror with a cut-off wavelength of 800 nm is used to separate the

transmitted Raman probe spectrum into the high- and low-frequency parts, which are then measured by two photodiodes (PD<sub>3</sub> and PD<sub>4</sub> in Figure S1a). The short-wavelength part of the fifth-order signal that is detected by PD<sub>3</sub> carries information on the GSA<sup>(5)</sup> signal, whereas the long-wavelength part of the signal detected by PD<sub>4</sub> corresponds to the ESA<sup>(5)</sup> signal. All the detected signals by PD<sub>1</sub>, PD<sub>2</sub>, PD<sub>3</sub>, and PD<sub>4</sub> are low-pass filtered at below 48 MHz ( $< f_r$ ) not only to suppress the repetition rate beat notes but also to record only the dual-ASOPS signals that depend on both  $t_1$  and  $t_2$ .

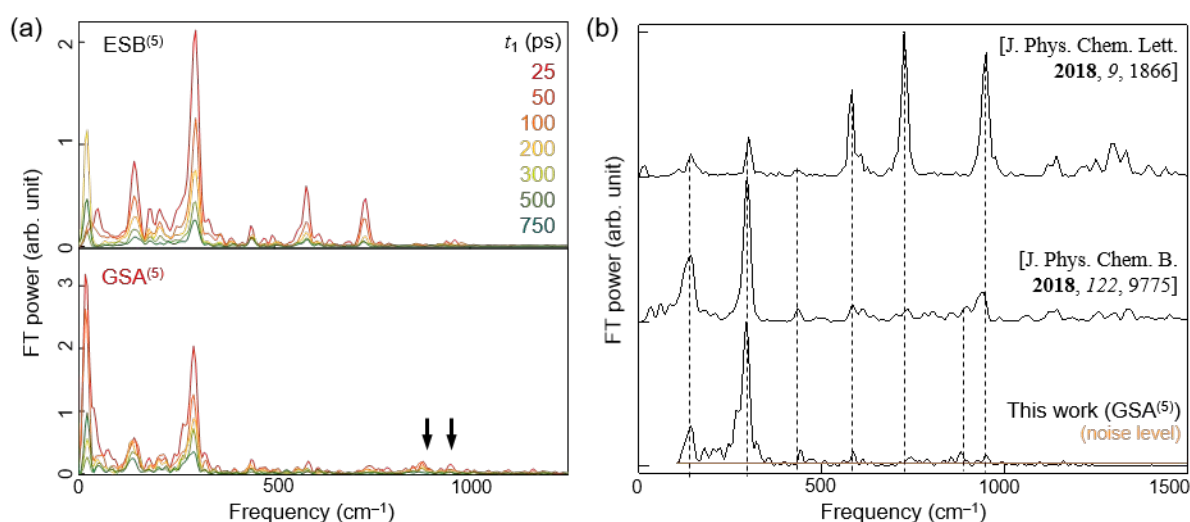


**Figure S2.** (a) Time-resolved Raman spectra (TRS) of IR125 in ethanol solution. In the upper (lower) panel, we show the waiting time-resolved Raman spectra extracted from the ESB<sup>(5)</sup> (GSA<sup>(5)</sup>) signals. (b) Impulsive resonant Raman spectra of IR125 reported in Refs. [1] (middle) and [2] (top) (Refs. [19] and [16] in the main text), and the TRS of GSA<sup>(5)</sup> at  $t_1 = 25$  ps. Noise level of the TRS is shown as an orange line.

The full-width-at-half-maximum (FWHM) of the cross-correlation function between the Raman pump and Raman probe pulses is measured to be 28 fs, which determines the ultimate time-resolution of our fifth-order STL-ISRS, where a 100- $\mu\text{m}$ -thick BBO crystal was put at the sample position to measure the cross-correlation. Although the pulse duration time of our MLs is 7 fs, the FWHM of cross-correlation intensity, 28 fs, is much broader than the pulse duration time. This deviation can be understood by noting that the spectrum of the ML<sub>2</sub> is narrowed by using a long-pass filter. However, still, the time-resolution of our system, which is 28 fs, is short enough to study the vibronic oscillations with frequencies of 875 and 950  $\text{cm}^{-1}$ , which appear in the STL-ISRS signal from IR125 solution (two arrows on GSA<sup>(5)</sup> in Figure S2a). The repetition

frequency detuning factors,  $\Delta f_r = 38.4$  Hz and  $\delta f_r = 77$  mHz, mean that the time intervals between the actinic pump and Raman pump pulses and between the Raman pump and Raman probe pulses are  $\Delta t_1 = 25.07$  ps and  $\Delta t_2 = 6$  fs, respectively. These parameters for the repetition frequency detuning factors were chosen both because we wanted to measure vibrational coherence whose period is shorter than 28 fs and because the uncertainty in determining the waiting time is approximately 10 ps (see Supporting Information Note 2 below).

Optical samples, IR125 and IR144, were purchased from Exciton and used for the STL-ISRS experiments without further purification. They are dissolved in ethanol, and the light absorbance of each solution sample is adjusted to be approximately 0.2 at the absorption maxima. The thickness of the sample cell is about 200  $\mu\text{m}$ . The thickness of the front window of the sample cell is as thin as 100  $\mu\text{m}$  so that we can ignore additional pulse broadening induced by the optical cell itself. A continuous flow of the sample solution is maintained during the STL-ISRS measurements, where a gear pump (Micropump) is used, and the flow rate is set to be 5 ml/s.

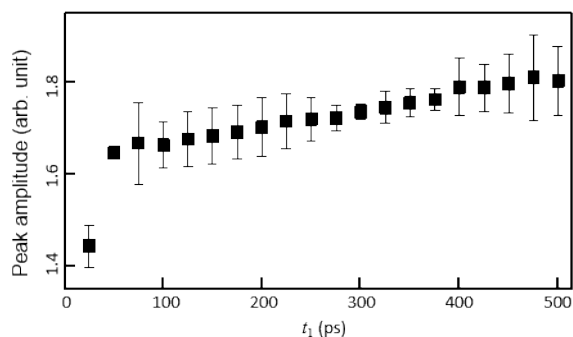


**Figure S3.** The waiting time  $t_1$ -dependence of the transient Raman peak at  $141\text{ cm}^{-1}$  in the ESB<sup>(5)</sup> signal from the IR144 ethanol solution. Data points are averaged over three independent measurements, where the error bars are standard deviations.

In our STL-ISRS, the peak amplitudes in the normalized time-resolved Raman spectrum (TRS) relative to the fifth-order signal intensity (Figure 3c in the main text) depend not only on the spectral shape (usually fixed during experiment) but also on the dumping conditions, e.g., the peak powers of the actinic and Raman pump pulses, the sample concentration, and the pulse spectra. To examine the waiting time  $t_1$ -dependence of the vibronic peak amplitude of the low-

frequency mode at  $141\text{ cm}^{-1}$ , we carried out three independent measurements, while all the experimental parameters are kept constant. Figure S3 plots the peak amplitude of the  $141\text{ cm}^{-1}$  vibronically excited mode versus waiting time. The statistical error (standard deviation) of each point is approximately 10 % of the corresponding peak amplitude at  $t_1 < 500\text{ ps}$ . It is clear that the peak amplitude of this low-frequency mode increases in time  $t_1$ , which indicates that the molecular structure slightly changes upon solvation by surrounding ethanol molecules.

## 2. Experimental details on how to control the two delay times

There are two time-delays in STL-ISRS, where the first one ( $t_1$ ) is the pulse-to-pulse time-delay between  $ML_1$  (actinic pump) and  $ML_2$  (Raman pump), and another ( $t_2$ ) is that between  $ML_2$  (Raman pump) and  $ML_3$  (Raman probe). To achieve the quasi-orthogonal time-delay generations of  $t_1$  and  $t_2$  with three different repetition rates, i.e.,  $t_1$  must be kept constant during the  $t_2$ -scan, one should carefully consider the timescales of spectroscopic observables and relaxation processes. In the STL-ISRS experiment,  $t_1$ -scanning is needed to monitor the population dynamics of photoexcited molecules that are subject to intra- and inter-molecular energy transfers, relatively slow solvation dynamics, and sometimes photochemical reactions that occur in the time range from picoseconds to several nanoseconds. On the other hand, the second delay time  $t_2$  needs to be scanned with a femtosecond time-interval for several picoseconds to measure the relaxations of vibrational wave packets created by the interaction of actinic pump-excited molecules with a subsequent ( $t_1$ -delayed) Raman pump pulse. Therefore, the required time resolutions for the  $t_1$  and  $t_2$  scans are significantly different from each other.

The automatic time-delay scanning of  $t_2$  is achieved with an ASOPS, where the scan range is rather short ( $< 10\text{ ps}$ ). In fact, we recently demonstrated that an ASOPS-based coherent vibrational spectroscopy with sub-10 fs time-resolution and a few picoseconds time-scanning is feasible.<sup>2</sup> Here, the detuning frequency ( $\Delta f_r$ ) between the repetition frequencies of  $ML_2$  and  $ML_3$  determines the speed of  $t_2$ -scan, and the time interval of  $t_2$ , denoted as  $\Delta t_2$ , is given by

$$\Delta t_2 = \left| \frac{1}{f_{r,2}} - \frac{1}{f_{r,3}} \right| = \frac{\Delta f}{f_r (f_r + \Delta f_r)} \cong \frac{\Delta f}{f_r^2}. \quad (\text{S1})$$

For  $\Delta f_r = 38.4$  Hz with  $f_r = 80$  MHz, we have  $\Delta t_2 = 6$  fs. For one cycle of  $t_2$ -scan, the number of Raman pump or probe pulses used is  $f_r/\Delta f_r$ , which is, in the present case, 2.08 million. We were able to estimate the standard error of the total scan time for the  $t_2$ -scan is 0.3 %, when we performed dual-frequency comb transient absorption experiments.<sup>2</sup> Therefore, the frequency resolution and standard error of the vibrational frequencies obtained from the Fourier transform of the ESB<sup>(5)</sup> and GSA<sup>(5)</sup> signals can be estimated, respectively, to be  $11 \text{ cm}^{-1}$  and  $0.35 \text{ cm}^{-1}$  for the  $141 \text{ cm}^{-1}$  mode.

Similar to  $t_2$ -scan, the time delay  $t_1$  between the actinic pump and Raman pump pulses can be automatically scanned through another ASOPS scheme with the constant difference ( $\delta f_r$ ) between the repetition frequencies of ML<sub>1</sub> and ML<sub>2</sub>. The time interval of the  $t_1$ , denoted as  $\delta t_1$ , is given by

$$\delta t_1 = \left| \frac{1}{f_{r,1}} - \frac{1}{f_{r,2}} \right| = \frac{\delta f_r}{(f_r + \Delta f_r + \delta f_r)(f_r + \Delta f_r)} \cong \frac{\delta f_r}{f_r^2}. \quad (\text{S2})$$

For  $\delta f_r = 77$  mHz with  $f_r = 80$  MHz, we have  $\delta t_1 = 12.03$  as. It should be emphasized that, for the present STL-ISRS measurements, we intentionally set  $\delta f_r$  to be approximately three orders of magnitude smaller than  $\Delta f_r$ . Therefore, as shown above,  $\delta t_1$  is similarly three orders of magnitude smaller than  $\Delta t_2$ . Among 2.08-million pairs of the Raman pump and probe pulses during one cycle of the  $t_2$  scanning, only the first several thousands of pairs of the Raman pump and probe pulses after  $t_2 = 0$ , which is the time when the Raman pump pulse overlaps with the Raman probe pulse in time domain, provide meaningful information on the STL-ISRS signal because the relaxation time of each vibrational coherence is on the order of picoseconds. Over a few picoseconds, the time slip between the actinic pump pulse and the Raman pump pulse is just a few femtoseconds, which is much less than  $\Delta t_1$ . Therefore, it is quite safe to assume that the waiting time  $t_1$  is nearly constant during a given  $t_2$ -scan range ( $< 10$  ps). This dual-ASOPS approach that allows us to record the STL-ISRS signals as functions of the two delay times in the time domain is immensely important for shortening the data acquisition time.

Now, after a single cycle of  $t_2$ -scan, which takes a time of  $1/\Delta f_r$  ( $= 26.04$  ms), the time delay between the actinic pump pulse and the Raman pump pulse is increased by  $\Delta t_1$ . Thus, the increment of  $t_1$  per single cycle of  $t_2$ -scan,  $\Delta t_1 = N_2 \delta t_1$ , becomes the time interval of the waiting time and can be estimated with the experimental parameters, where  $N_2$  is the number of Raman probe pulses over the time of  $1/\Delta f_r$ , as

$$\Delta t_1 = N_2 \delta t_1 = \frac{1/f_r}{\Delta t_2} \frac{\delta f_r}{f_r^2} = \frac{f_r}{\Delta f_r} \frac{\delta f_r}{f_r^2} = \frac{\delta f_r}{\Delta f_r \cdot f_r}. \quad (\text{S3})$$

For  $\Delta f_r = 38.4$  Hz and  $\delta f_r = 77$  mHz with  $f_r = 80$  MHz, we have  $\Delta t_1 = 25.07$  ps. This time interval for  $t_1$  is sufficiently short enough to study slow processes like photochemical reactions during the waiting time after the photoexcitation by an actinic pump pulse.

Since a complete two-dimensional ( $t_1, t_2$ )-dependent STL-ISRS data set can be recorded in a single  $t_1$ -scan time ( $1/\delta f_r = 13$  s in the present work), STL-ISRS is capable of collecting a large number of data points efficiently compared to FSRS and TR-ISRS. Although it is not easy for us to compare the data acquisition efficiencies of these three techniques directly because of the differences in laser systems, signal-to-noise ratios, detectors, and optical layouts, ignoring all the other experimental parameters, we could approximately estimate the relative data acquisition times for FSRS ( $T_{\text{DAQ,FSRS}}$ ), TR-ISRS ( $T_{\text{DAQ,TR-ISRS}}$ ) and STL-ISRS ( $T_{\text{DAQ,STL-ISRS}}$ ) as follows,

$$T_{\text{DAQ,FSRS}} = T_{2,A} \times N_1 \quad (T_{2,A} : \text{data acquisition time of array-type detector} + \text{dead time})$$

$$T_{\text{DAQ,TR-ISRS}} = T_{2,S} \times N_2 \times N_1 \quad (T_{2,S} : \text{data acquisition time of single-point detector} + \text{dead time})$$

$$T_{\text{DAQ,STL-ISRS}} = 1/\delta f_r \quad (13 \text{ s } (\delta f_r = 77 \text{ mHz and } N_{1,\text{max}} = 500) \text{ in the present work}).$$

Here,  $N_1$  and  $N_2$  are the numbers of  $t_1$  and  $t_2$  data points. Dead time means the time required to prepare the next data recording e.g., travel time of a motorized stage used. According to the above equations, STL-ISRS is found to be advantageous if one needs to make a wide dynamic range measurement of the  $t_1$ -scan with large  $N_1$ . However, the STL-ISRS is not superior over FSRS and TR-ISRS in terms of data acquisition speed, if the photoexcited molecules of interest can recover back to their initial ground state rapidly.

Note that the uncertainties of the two time-intervals ( $\Delta t_1$  and  $\Delta t_2$ ) should be carefully examined before setting the experimental parameters. The timing jitter after a single scanning of

the  $t_2$ -delay time,  $\delta(\Delta t_1)$ , can be estimated from the optical cross-correlation signal and measured to be approximately  $\delta(\Delta t_2) \sim 5$  fs. This small timing jitter results from our tight synchronization of the repetition rates of the three MLs as described in Supporting information 1. The accumulated timing error (jitter) of  $\delta(\Delta t_1)$  can be calculated from the error propagation law as  $\delta(\Delta t_1) = \sqrt{N_2} \delta(\Delta t_2) \sim 7$  ps, which is consistent with the experimental observation of 10 ps. Here,  $\delta(\Delta t_1)$  was measured from the standard deviation of the time difference between the two cross-correlation signals at a fixed  $t_1$ , which could be achieved by setting  $f_{r,1} = f_{r,2}$  experimentally. More specifically, the sum-frequency generation (SFG) signals between ML<sub>1</sub> and ML<sub>3</sub> and between ML<sub>2</sub> and ML<sub>3</sub> are generated by a BBO crystal placed at the sample position during the  $t_2$ -scan. Then, a series of two non-collinear SFG signals are detected per each cycle of  $t_2$ -scan with a single photodiode (PD), where the repetition rates of the three MLs satisfy the relation  $f_{r,1} = f_{r,2} = f_{r,3} - \Delta f_r$ . The cross-correlation signal between ML<sub>1</sub> and ML<sub>3</sub> provides the trigger (reference) signal for the fast digitizer, which sets the time zero, and the time delay from the time zero to the cross-correlation signal resulting from the overlap of pulses from ML<sub>2</sub> and ML<sub>3</sub> is measured. We found no notable long-time drift of the time delay, while its standard deviation, i.e.  $\delta(\Delta t_1)$ , turns out to be approximately 10 ps.

### 3. Optical triggering scheme

Optical triggering is a prerequisite for achieving both femtosecond time-resolution and accurate time-zero positioning in ASOPS-based time-resolved spectroscopy.<sup>1</sup> In our STL-ISRS experiment, approximately a half of the laser powers from ML<sub>2</sub> and ML<sub>3</sub> is separated and non-collinearly focused into a 100- $\mu\text{m}$ -thick BBO crystal with the optic axis of  $29.2^\circ$  to generate the cross-correlation (SFG) signal. The FWHM of the cross-correlation intensity is found to be 12.5 fs, which is much shorter than the time resolution of our STL-ISRS (28 fs). Because the  $t_1$  time step should be larger than the estimated uncertainty of 10 ps, the measured cross-correlation signal, whose pulse duration is 28 fs in FWHM, between ML<sub>1</sub> and ML<sub>2</sub> is short enough for the stable triggering of the whole experiment.

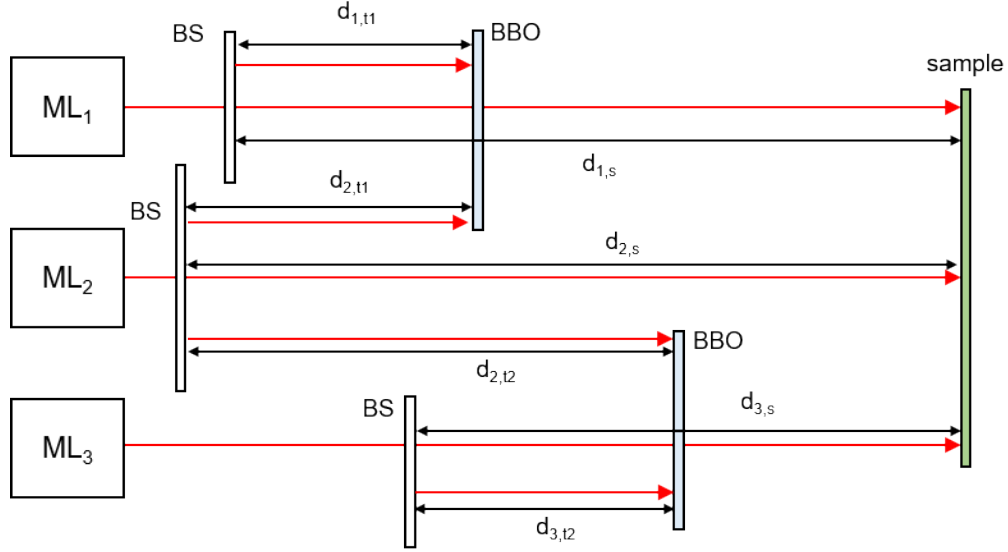


**Figure S4.** Schematic diagram representing the relative optical path lengths of the pulse trains from  $ML_1$ ,  $ML_2$ , and  $ML_3$ . The three beam splitters in this figure correspond to those in Figure S1a. Likewise, the short- and long-pass filters in this figure are those in Figure S1a. BBO represents beta-barium borate crystal

Another critical issue in the general femtosecond time-resolved spectroscopy experiments is the repeatability of time scanning. In our STL-ISRS, the accuracy and stability of the optical trigger determine the position accuracy of the time zeros for a dual-ASOPS based experiment. The time-zeros of  $t_1$  and  $t_2$  are determined by the relative positions of the optical-trigger-generating nonlinear crystals (BBOs in Figure S1a) and the optical sample, and they are adjustable experimentally by displacing the relative positions between them. Figure S4 illustrates the relative optical path lengths between the corresponding lasers and the sample. The time delays between the  $t_1$ -trigger signal and the time zero of  $t_1$  ( $t_1 = 0$ ) and between the  $t_2$ -trigger signal and  $t_2 = 0$ , which are denoted as  $\delta t_1$  and  $\delta t_2$ , respectively, are given by

$$\delta t_1 = \frac{(d_{1,s} - d_{1,t1}) - (d_{2,s} - d_{2,t1})}{c} \quad \text{and} \quad \delta t_2 = \frac{(d_{2,s} - d_{2,t2}) - (d_{3,s} - d_{3,t2})}{c}. \quad (\text{S4})$$

It should be noted that the optical path lengths between beam splitters on the path and the corresponding BBO crystals generating trigger signals and those between beam splitters and the optical sample (see Figure S4) could be different from one another.  $\delta t_2$  should be set to zero experimentally to minimize the effect of  $\Delta t_2$  fluctuation caused by the repetition rate fluctuation. In fact, the repetition rate fluctuation, which is related to the response time of a piezo translator

controlling the cavity length of a given ML, is negligible if the desired scan range is less than tens of ps.<sup>1</sup> The time-delays expressed in Eq. (S4) are however ideal values so that the uncertainties in determining the time-delays are to be considered. Here, the uncertainty in  $\delta t_2$  is mainly determined by two factors. One of them is the rise time of the fast digitizer, but it is usually not a critical factor if the clocks for the trigger and data channels are stabilized. Another factor is the positioning accuracy of the optomechanics. On the other hand, the uncertainty in  $\delta t_1$  should be more carefully minimized than that in  $\delta t_2$ , because we use two data recorders, i.e., slow and fast digitizers in Figure S1a, with a single data acquisition software (LabView in our experiment). To perform a coherent averaging of STL-ISRS signals, every  $t_1$ -scan should start at a fixed time-delay after each  $t_1$ -trigger signal. However, it is nearly impossible to achieve such an accurate control of  $t_1$  scanning because the response time of the software is fairly slow, as explained above. In the present work, the timing error caused by the software is estimated to be 30 ms, which corresponds to the uncertainty of 30 ps for  $\delta t_1$  in our experimental condition. Thus,  $\delta t_1$  should be sufficiently longer than the uncertainty (30 ps) in  $\delta t_1$  to avoid any loss of data during the compensation process for the displaced signals due to the software timing uncertainty (30 ms). This experimental adjustment is necessary for the coherent averaging of STL-ISRS data (see Supporting Information 4 for details on this compensation process).

#### 4. Data processing for STL-ISRS

Figure S5 schematically shows a data acquisition procedure for the STL-ISRS. The optical trigger generated by the temporal overlap between pulses from ML<sub>2</sub> and ML<sub>3</sub> defines the time zero of  $t_2$  at a given waiting time  $t_1$ . The STL-ISRS signals (green line in Figure S5) are detected by PD<sub>3</sub> and PD<sub>4</sub> (Figure S1), while the  $t_2$ -trigger signal is detected by PD<sub>1</sub> (see Figure S1). The upper panels are the detected signals at  $t_{\text{lab}} = 0$  and  $1/\Delta f_r$ , where the optical trigger precedes the actinic pump pulse. Therefore, the measured signal contains only the third-order signal induced by the Raman pump and probe pulses. In the third panel, all three pulses from the three MLs overlap in time so that both the third- and fifth-order signals contribute to the detected signal. In this case, it is difficult to measure the fifth-order signal selectively. The bottom two panels are the cases that the actinic pump pulse interacts with the sample first and then followed by the Raman pump and Raman probe pulses from ML<sub>2</sub> and ML<sub>3</sub>. In these cases, the signals in

the negative time domain are dictated by the third-order signal, but both the third- and fifth-order terms contribute to the signal in the positive time domain in Figure S5. We collect data within a time window (red box) shown in Figure S5, where the signal contains data in both the negative and positive time domains. To obtain the desired fifth-order signal, we need to subtract the third-order signal from the total signal. The range of data collecting time is from -0.25 ps to +2.75 ps. Here, it should be noted that the vibrational dephasing time is on the order of a few picoseconds, and the time required for the complete recovery of the photoexcited molecules is less than 300 ps for the IR144 in ethanol solution.

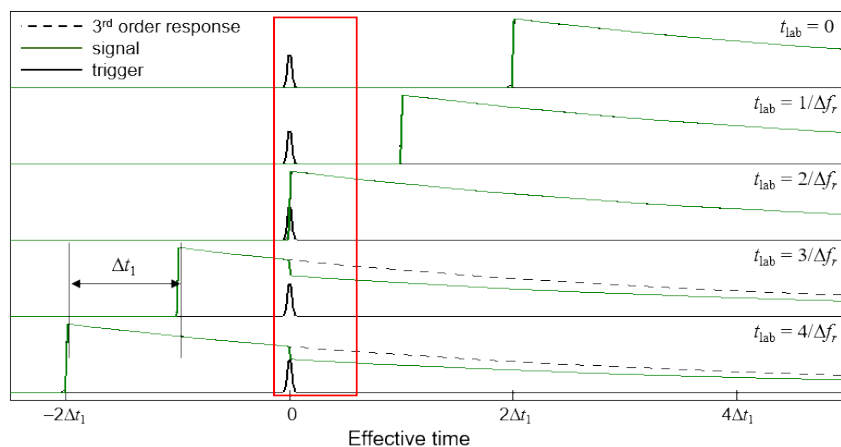


**Figure S5.** Timing sequence between the optical trigger (black) between  $ML_2$  and  $ML_3$  and simulated STL-ISRS signal (green) detected by the fast digitizer at two different channels. The red box represents the data recording window of the STL-ISRS signals defined relative to the optical trigger signal at each  $t_1$ -step. ( $t_{lab}$ : laboratory time)

After taking a series of data points in a one-dimensional array form, where the numbers of data points for the  $t_1$ - and  $t_2$ -scans are denoted as  $N_1$  and  $N_2$ , respectively, it is necessary to convert the one-dimensional data into a matrix form depending on the  $t_1$  and  $t_2$  times (see Supporting Reference 1 for details). Once the raw array data is converted into a two-dimensional  $N_1 \times N_2$  matrix form, one can obtain the TRS by Fourier transforming the data with respect to  $t_2$ . For statistical averaging, we carried out multiple measurements. The multiple data sets of STL-ISRS, however, cannot be averaged to increase the signal-to-noise ratio due to the time jitter of  $t_1$ , which is associated with the finite response time of the data acquisition software and was estimated to be approximately 30 ps in the present work. For coherent signal averaging over 1000 data sets, we numerically shift the data index related to  $t_1$  to have uncertainty smaller than  $\Delta t_1$  (25 ps).

## 5. Bi-exponential fitting

Nonlinear least-square fitting analyses of the fifth-order signals was performed. More specifically, the  $t_2$ -trace at each  $t_1$  point,  $y(t_1, t_2)$ , shown in Figure 2c is fitted with a bi-exponential function,  $f(t_1, t_2)$ , given by

$$f(t_1, t_2) = a_{bg}(t_1) + a_0(t_1) + \sum_{n=1,2} a_n(t_1) \exp[-t_2/\tau_n(t_1)]. \quad (\text{S5})$$

where  $a_{bg}$  is the mean value at  $t_2 < -100$  fs, and the other constants,  $a_0$ ,  $a_n$ , and  $\tau_n$ , are the fitting parameters. The data at  $t_2 < 100$  fs were not included in the bi-exponential fitting analysis to remove the convolution effect near  $t_2 = 0$ . Figure S5 shows the fitting results. The residual signals, which is the difference between the raw data,  $y(t_1, t_2)$ , and the fitted bi-exponential function,  $f(t_1, t_2)$ , are plotted in Figure 3c. Note that these residual signals show the vibration coherences clearly.

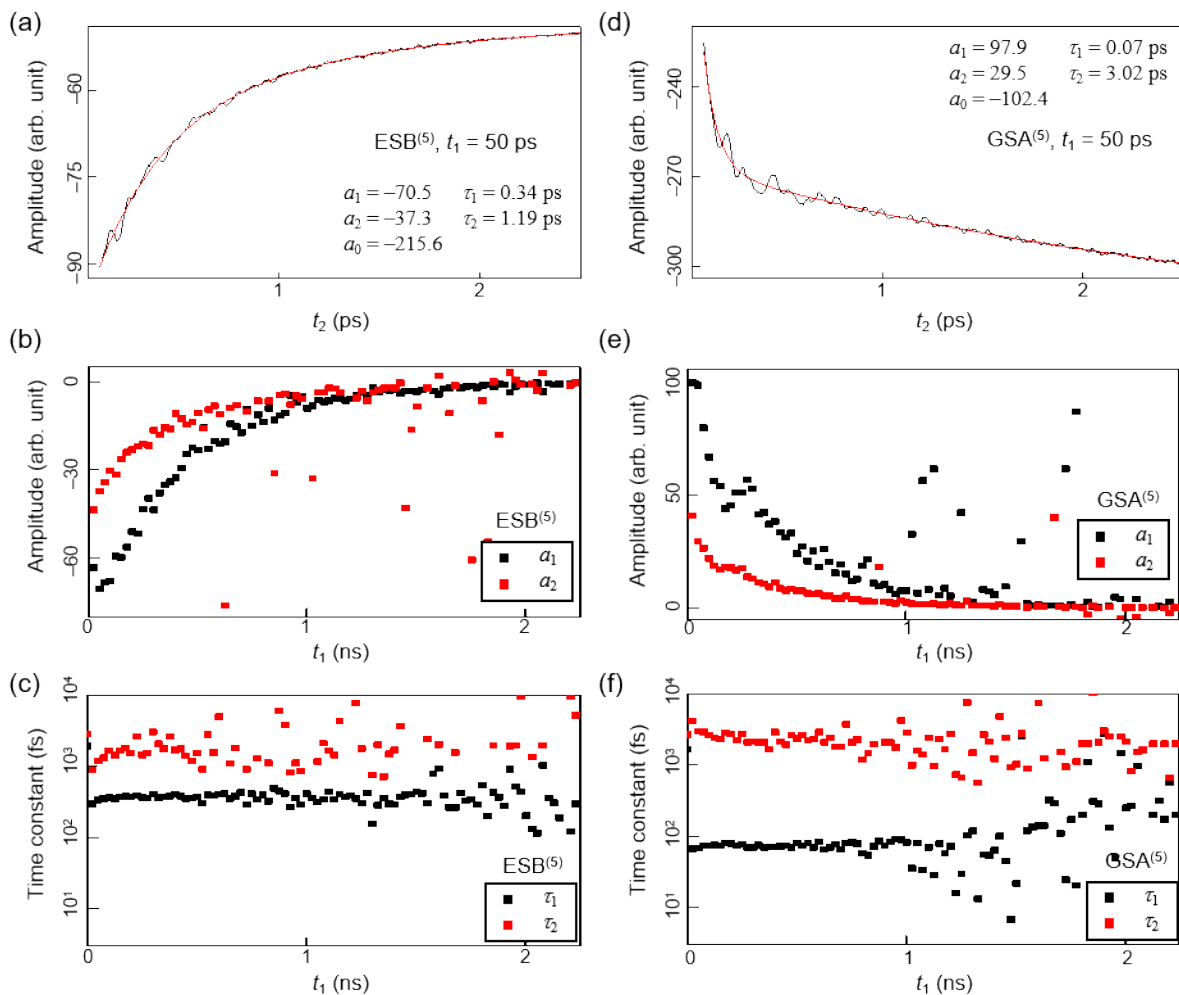


**Figure S6.** Bi-exponential fitting analysis results for the  $t_2$ -traces of ESB<sup>(5)</sup> and GSA<sup>(5)</sup> that are shown in Figure 2c. The fitting results for the ESB<sup>(5)</sup> and GSA<sup>(5)</sup> signals at  $t_1 = 50$  ps are shown in (a) and (d), respectively. The optimized fitting parameters are given in each panel. Note that those fitting parameters depend on  $t_1$  and they are plotted in (b), (c), (e), and (f) with respect to  $t_1$ .

## Supporting References

- (1) Kim, J.; Yoon, T. H.; Cho, M. Interferometric measurement of transient absorption and refraction spectra with dual frequency comb. *J. Phys. Chem. B* **2018**, *122*, 9775-9785.
- (2) Kim, J.; Cho, B.; Yoon, T. H.; Cho, M. Dual-frequency comb transient absorption: broad dynamic range measurement of femtosecond to nanosecond relaxation processes. *J. Phys. Chem. Lett.* **2018**, *9*, 1866-1871.